Original Article

Predicting *MET* exon 14 skipping mutation in pulmonary sarcomatoid carcinoma by whole-tumour texture analysis combined with clinical and conventional contrast-enhanced computed tomography features

Lei Miao[1#], Tian Qiu[2#], Yan Li[2#], Jianwei Li[1], Xu Jiang[1], Mengwen Liu[1], Xue Zhang[1], Jiuming Jiang[1], Huanhuan Zhang[1], Yanmei Wang[3], Xiao Li[4], Jianming Ying[2], Meng Li[1]

[1]Department of Radiology, National Cancer Center/National Clinical Research Center for Cancer/Cancer Hospital, Chinese Academy of Medical Sciences and Peking Union Medical College, Beijing, China; [2]Department of Pathology, National Cancer Center/National Clinical Research Center for Cancer/Cancer Hospital, Chinese Academy of Medical Sciences and Peking Union Medical College, Beijing, China; [3]GE Healthcare China, Pudong New Area, Shanghai, China; [4]Department of Interventional Therapy, National Cancer Center/National Clinical Research Center for Cancer/Cancer Hospital, Chinese Academy of Medical Sciences and Peking Union Medical College, Beijing, China

Contributions: (I) Conception and design: L Miao, M Li; (II) Administrative support: M Li, J Ying, X Li; (III) Provision of study materials or patients: L Miao, T Qiu, Y Li, (IV) Collection and assembly of data: L Miao, J Li, X Jiang, M Liu, X Zhang, J Jiang, H Zhang; (V) Data analysis and interpretation: L Miao, Y Wang; (VI) Manuscript writing: All authors; (VII) Final approval of manuscript: All authors.

[#]These authors contributed equally to this work as co-first authors.

Correspondence to: Xiao Li, MD. Department of Interventional Therapy, National Cancer Center/National Clinical Research Center for Cancer/Cancer Hospital, Chinese Academy of Medical Sciences and Peking Union Medical College, 17 Panjiayuan Nanli, Chaoyang District, Beijing 100021, China. Email: simonlixiao@gmail.com; Jianming Ying, MD. Department of Pathology, National Cancer Center/National Clinical Research Center for Cancer/Cancer Hospital, Chinese Academy of Medical Sciences and Peking Union Medical College, 17 Panjiayuan Nanli, Chaoyang District, Beijing 100021, China. Email: jmying@cicams.ac.cn; Meng Li, MD. Department of Radiology, National Cancer Center/National Clinical Research Center for Cancer/Cancer Hospital, Chinese Academy of Medical Sciences and Peking Union Medical College, 17 Panjiayuan Nanli, Chaoyang District, Beijing 100021, China. Email: lmcams@163.com.

Background: Pulmonary sarcomatoid carcinoma (PSC) is a rare, highly malignant type of non-small cell lung cancer (NSCLC) with a poor prognosis. Targeted drugs for *MET* exon 14 (*MET*ex14) skipping mutation can have considerable clinical benefits. This study aimed to predict *MET*ex14 skipping mutation in PSC patients by whole-tumour texture analysis combined with clinical and conventional contrast-enhanced computed tomography (CECT) features.

Methods: This retrospective study included 56 patients with PSC diagnosed by pathology. All patients underwent CECT before surgery or other treatment, and both targeted DNA- and RNA-based next-generation sequencing (NGS) were used to detect *MET*ex14 skipping mutation status. The patients were divided into two groups: *MET*ex14 skipping mutation and nonmutation groups. Overall, 1,316 texture features of the whole tumour were extracted. We also collected 12 clinical and 20 conventional CECT features. After dimensionality reduction and selection, predictive models were established by multivariate logistic regression analysis. Models were evaluated using the area under the curve (AUC), and the clinical utility of the model was assessed by decision curve analysis.

Results: *MET*ex14 skipping mutation was detected in 17.9% of PSCs. Mutations were found more frequently in those (I) who had smaller long- or short-axis diameters (P=0.02, P=0.01); (II) who had lower T stages (I, II) (P=0.02); and (III) with pseudocapsular or annular enhancement (P=0.03). The combined model based on the conventional and texture models yielded the best performance in predicting *MET*ex14 skipping mutation with the highest AUC (0.89). The conventional and texture models also had good performance (AUC =0.83 conventional; =0.88 texture).

Conclusions: Whole-tumour texture analysis combined with clinical and conventional CECT features may serve as a noninvasive tool to predict the *MET*ex14 skipping mutation status in PSC.

Keywords: Pulmonary sarcomatoid carcinoma (PSC); *MET* exon 14 skipping (*MET*ex14 skipping); texture analysis; computed tomography (CT)

Submitted Jan 16, 2024. Accepted for publication May 07, 2024. Published online Jun 11, 2024.
doi: 10.21037/tlcr-24-56
View this article at: https://dx.doi.org/10.21037/tlcr-24-56

Introduction

Pulmonary sarcomatoid carcinoma (PSC) is a rare, highly malignant type of non-small cell lung cancer (NSCLC) with a poor prognosis; it has a 0.3–1% incidence rate of all lung cancers (1-3). Although surgery is currently considered the primary treatment for PSC and some conventional chemotherapy regimens can be applied, their efficacy is limited (3-5). Excitingly, NSCLC has recently seen tremendous clinical benefits and improved patient outcomes from targeted therapy (6-9), which also provides new opportunities for therapeutic strategies in PSC. In recent studies, the frequency of *MET* exon 14 skipping (*MET*ex14 skipping) mutations appears to be much more prevalent in PSC (approximately 13–22%) (10-12). At the same time, several high-quality clinical studies have suggested that targeted drugs for *MET*ex14 skipping mutation (e.g., savolitinib, capmatinib, tepotinib, and crizotinib) can have considerable clinical benefits (1,13-15). Therefore, the accurate judgement of *MET*ex14 skipping mutations in PSC patients is critical for individualized treatment selection.

Advanced unresectable or fragile PSC patients require a biopsy to identify the pathological type and *MET*ex14 skipping mutation status, but PSC is usually large in size and mixed in components. Biopsy may not be performed, and false negative results may also be obtained (12,16-18). Meanwhile, the occurrence of *MET*ex14 skipping mutation is low, and the diverse compositions of the *MET*ex14 splice sites and their variable locations in intronic regions require examination by high-throughput sequencing or genotyping technologies (12). These are cost-inefficient for both hospitals and patients. Therefore, a noninvasive, convenient, and more reliable way of detecting *MET*ex14 skipping mutations in PSC patients is needed.

Computed tomography (CT) is the most used tool for detecting and diagnosing lung cancer, and contrast-enhanced computed tomography (CECT) can better reflect the tumour blood supply and contrast between tissues (19,20). Recent studies have investigated some clinical features or conventional CT/CECT features associated with *MET*ex14 skipping mutations in NSCLC (11,21,22), but only a very small number of PSC patients were included in these studies. Meanwhile, texture analysis or radiomics signatures, which can deeply reflect the heterogeneity of tumours, have been widely used in predicting gene mutations in lung cancer, such as epidermal growth factor receptor (EGFR), anaplastic lymphoma kinase (ALK), and Kirsten rat sarcoma viral oncogene homolog (KRAS) (23-27); however, none have been used for *MET*ex14 skipping mutations. Therefore, based on more PSC patients, our study tried to predict *MET*ex14 skipping mutations by whole-tumour texture analysis combined with clinical and CECT features. To the best of our

Highlight box

Key findings

- This study proposed a noninvasive and efficient method to predict *MET* exon 14 (*MET*ex14) skipping mutation in pulmonary sarcomatoid carcinoma (PSC) patients by whole-tumour texture analysis combined with clinical and conventional contrast-enhanced computed tomography (CECT).

What is known and what is new?

- Previous studies have attempted to predict epidermal growth factor receptor, anaplastic lymphoma kinase, and Kirsten rat sarcoma viral oncogene homolog mutations in non-small cell lung cancer patients through radiomics or conventional imaging features.
- We applied a similar approach to predict *MET*ex14 skipping mutation in PSC patients and proposed PSC patient-specific CECT imaging features, such as pseudocapsular or annular enhancement.

What is the implication, and what should change now?

- Using our predictive model to estimate *MET*ex14 skipping mutation in PSC patients can have considerable clinical benefits. Future studies should focus on validating these results in larger populations and exploring the potential application of these findings.

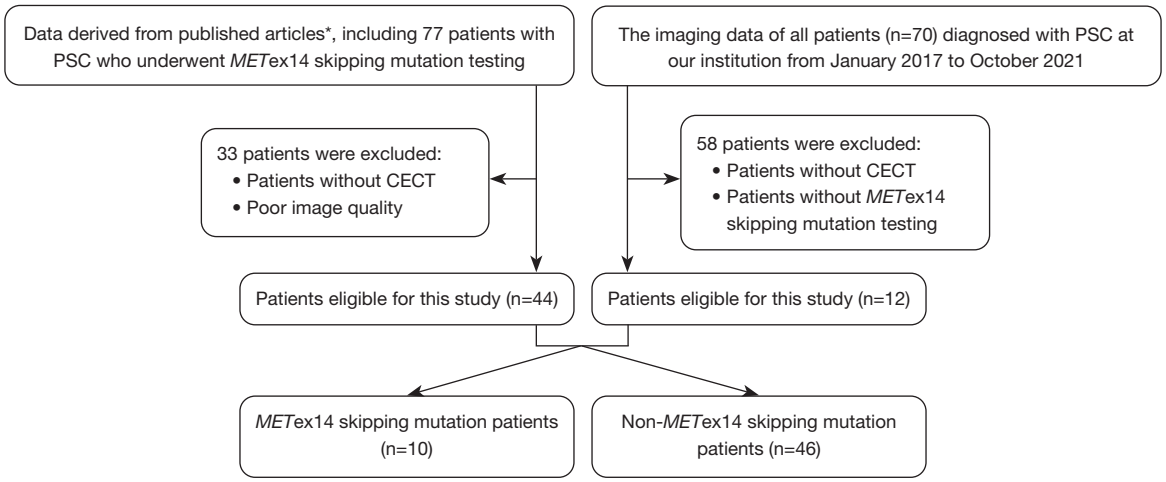

Figure 1 Flow diagram of the study cohort. *, Yang Z, Xu J, Li L, *et al.* Integrated molecular characterization reveals potential therapeutic strategies for pulmonary sarcomatoid carcinoma. *Nat Commun* 2020;11:4878; Li Y, Gao L, Ma D, *et al.* Identification of *MET* exon14 skipping by targeted DNA- and RNA-based next-generation sequencing in pulmonary sarcomatoid carcinomas. *Lung Cancer* 2018;122:113-9. PSC, pulmonary sarcomatoid carcinoma; *MET*ex14 skipping, *MET* exon 14 skipping; CECT, contrast-enhanced computed tomography.

knowledge, there have been no imaging studies on PSC in a large number of patients. Our study findings will also have implications for diagnosing PSC using conventional imaging. We present this article in accordance with the TRIPOD reporting checklist (available at https://tlcr.amegroups.com/article/view/10.21037/tlcr-24-56/rc).

Methods

Patient information

In this study, we reviewed the imaging data of all patients (n=77) based on a previously published study (12) and excluded patients (n=33) without CECT images or standard images. We reviewed the imaging data of all patients (n=70) diagnosed with PSC at the Cancer Hospital, Chinese Academy of Medical Sciences from January 2017 to October 2021 and excluded patients (n=58) without *MET*ex14 skipping mutation tests or CECT images. Thus, 56 patients were included in this study and divided into two groups: the *MET*ex*14* skipping mutation group and the nonmutation group.

The following inclusion criteria were applied: (I) pathological diagnosis of PSC; (II) *MET*ex14 skipping mutation status was detected by using targeted DNA- and RNA-based next-generation sequencing (NGS); (III) no clinical treatments, such as chemotherapy, were administered prior to the *MET*ex14 skipping mutation test; and (IV) CECT was performed before surgery or treatment, and the image quality was good. The exclusion criteria were as follows: (I) no *MET*ex14 skipping mutation test; (II) missing CECT images before surgery or other treatment; and (III) poor image quality. The study was conducted in accordance with the Declaration of Helsinki (as revised in 2013). The Ethical Committee of the Cancer Hospital, Chinese Academy of Medical Sciences approved this study approved this retrospective study (No. 18-224/1782) and waived the requirement for obtaining informed consent from patients, as data were de-identified, involving no potential risk to patients and no link between the patients and researchers. The flow diagram of the study cohort is shown in *Figure 1*.

METex14 skipping mutation analysis

All patients in the study received diagnoses of PSC confirmed through independent evaluations of hematoxylin and eosin (H&E) stained sections by two pathologists. The tissue samples were preserved using formalin fixation and embedded in paraffin for analysis. DNA- and RNA-based NGS was performed to test *MET*ex14 skipping mutations in tumour samples. Briefly, DNA and RNA extractions were performed using TIANamp Genomic DNA Kit (Tiangen, Beijing, China) and RecoverAll™ Total Nucleic Acid Isolation Kit for FFPE (Thermo Fisher Scientific, Waltham,

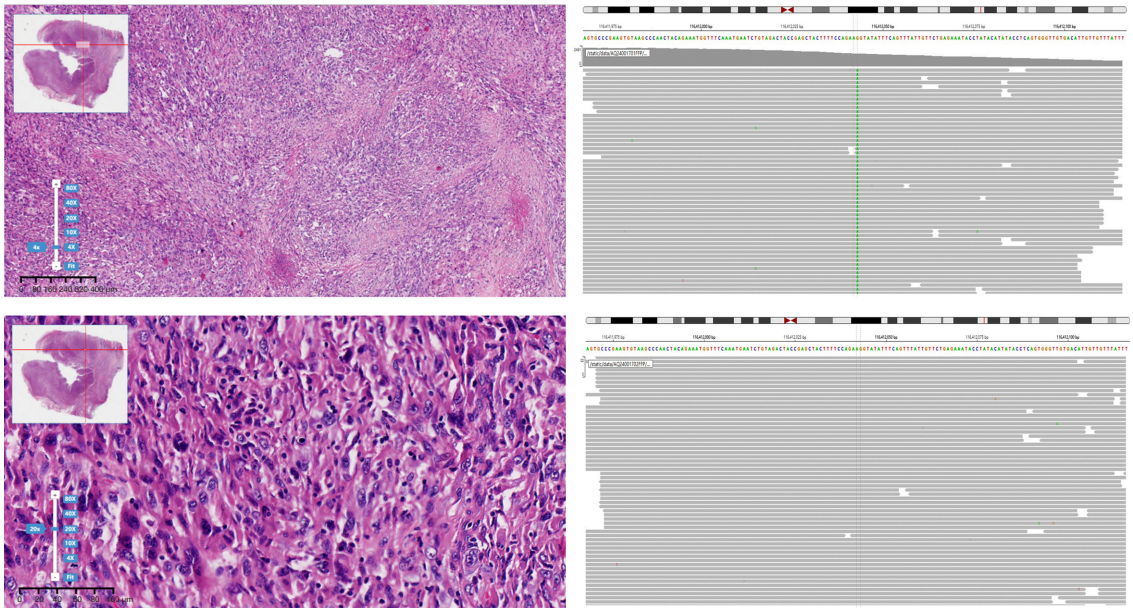

Figure 2 Representative H&E morphology and DNA-based NGS results of one *MET*ex14 skipping mutation case and one nonmutation case. H&E, hematoxylin and eosin; NGS, next-generation sequencing; *MET*ex14, *MET* exon 14.

MA, USA), respectively. Qubit quantitation platform was used to quantitate DNA and RNA concentration.

NGS based on DNA was conducted utilizing a tailor-made gene panel that includes the *MET* gene along with 17 additional oncogenes. DNA libraries were prepared and targeted NGS was performed as previously reported (12). A custom-crafted probe panel encompassing the junction of MET exons 13 to 15 was employed for the execution of RNA-based NGS. RNA libraries were prepared and the amplicon libraries were sequenced with an Ion Torrent Systems Proton system as previously reported (12). Representative H&E morphology and DNA-based NGS results of one *MET*ex14 skipping mutation case and one nonmutation case are shown in *Figure 2*.

Image acquisition

The image acquisition is described in supplementary material (Appendix 1).

Collection of clinical data and evaluation of conventional CECT features

Clinical data were collected through the Hospital Information System (HIS), including the following 12 characteristics: sex, age, smoking history, T stage, N stage, M stage, American Joint Committee on Cancer (AJCC) stage, location-lobe, location-distribution, translobar growth, long-axis diameter, and short-axis diameter. The clinical stage was determined according to the 8th edition of the AJCC guidelines for NSCLC staging.

All CECT images were evaluated by two radiologists (with three and 10 years of thoracic imaging diagnosis experience) who were blinded to the clinical data. The results were then confirmed by a chief physician specializing in thoracic imaging diagnosis. In cases of disagreement, a consensus was reached through consultation. Twenty CECT features were assessed, including shape, lobulation, margin, spiculation, texture, calcification, air bronchogram, bubble-like lucency, cystic change or necrosis, obstructive change, enhancement heterogeneity, pseudocapsular or annular enhancement, overall CECT value, CECT value of back muscle in the same slice, enhancement relative ratio, enhancement degree, pleural attachment, pleural retraction, pleural effusion, and lymphadenopathy. The definitions and scoring rules of the conventional CECT features are described in Table S1.

Tumour segmentation

The whole tumour was manually delineated slice-by-slice by two radiologists (with 3 and 10 years of lung cancer imaging

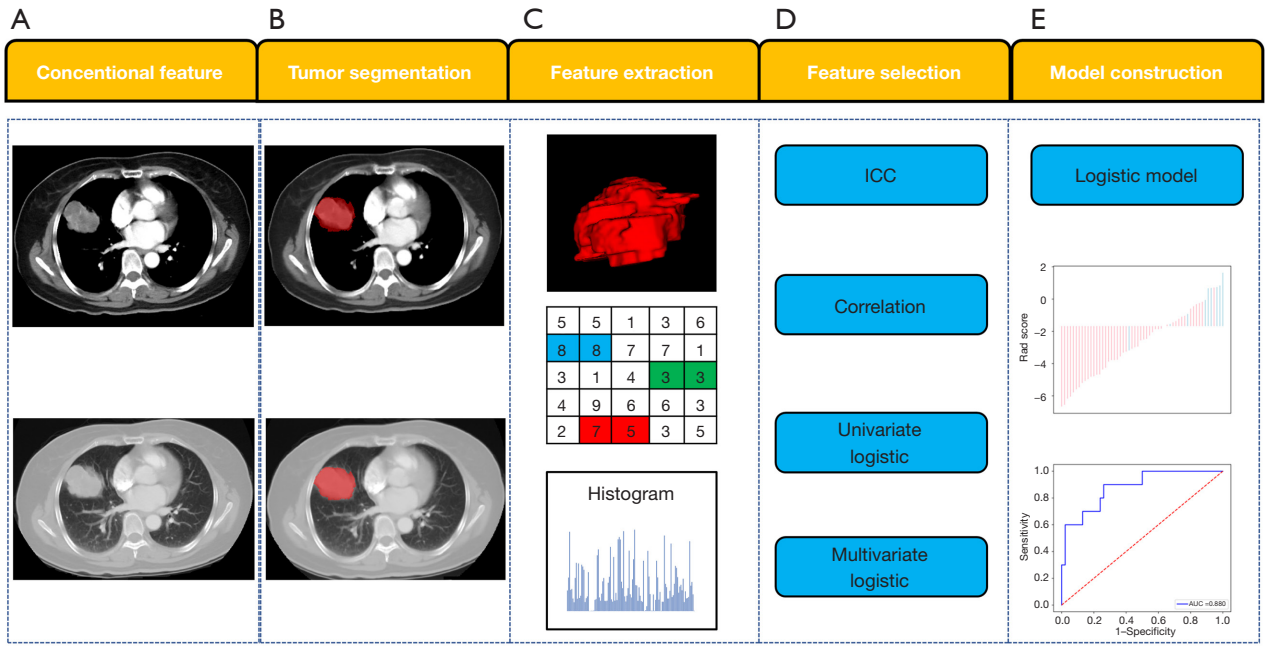

Figure 3 Workflow of texture analysis. In module E, the bar graph shows the predicted values of model according to the ranking, with red and blue corresponding to the predicted values of non-mutations and mutations, respectively. ICC, intraclass correlation coefficient; AUC, area under the curve.

diagnosis experience) in the lung window setting [width 1,200 Hounsfield unit (HU), level −500 HU] and mediastinal window (width 350 HU, level 50 HU) by using ITK-SNAP (version 2.2.0, www.itksnap.org) software and reviewed by an expert radiologist with 20 years of lung cancer imaging diagnosis experience. The radiologists were blinded to the patients' clinical and pathological details. The volume of interest (VOI) was drawn according to the tumour-lung interface, excluding vasculature, bronchus, atelectasis, lymph nodes, consolidation or obstructive changes in the lung, and other adjacent normal tissues as much as possible.

Feature extraction

First, all CECT images were preprocessed by resampling to 1×1×1 (mm^3) before VOI delineation to eliminate differences between images with different slice thicknesses. Then, all CECT images were normalized with Z scores to obtain a standard normal distribution of image intensities. Texture features were extracted from the VOIs by using AK software (Analysis Kit, GE Healthcare, Chicago, IL, USA). Each image had 1,316 texture features, including 14 shape features (3D), 18 first-order features, 24 grey level co-occurrence matrix (GLCM) features, 16 grey level run length matrix (GLRLM) features, 16 grey level size zone matrix (GLSZM) features, 14 grey level dependence matrix (GLDM) features, 5 neighbouring grey tone difference matrix (NGTDM), 744 wavelet transform features (using the PyWavelets package), 186 Laplacian of Gaussian (LoG) features (based on SimpleITK functionality), and 279 local binary patterns (LBPs). All texture features were obtained from open-source PyRadiomics (http://www.radiomics.io/pyradiomics.html) as recommended by the Image Biomarker Standardisation Initiative (IBSI) (28). The processes of tumour segmentation and feature extraction are shown in *Figure 3*.

Feature selection and model construction

Data reduction and feature selection processes were performed to select the most relevant features for constructing the models. First, the correlation test between features was assessed. Some features with high correlation (r>0.8) were further evaluated for the diagnostic performance of predictive targets, and the features with higher area under the curve (AUC) were retained. Based on the above methods, the texture features with high diagnostic efficacy and low correlation between features

(r<0.8) can be screened out. Second, we used univariate logistic regression to eliminate irrelevant features, and features with P<0.05 were selected. Finally, multivariate logistic regression analysis was used to select the most significant features, and the texture model was established. The differences in clinical/conventional features between the *MET*ex14 skipping mutation and nonmutation groups were compared using univariate analysis, and features with P<0.05 were selected. Multivariate logistic regression analysis was used to select the most significant features, and the conventional model was established. The combined model was established by combining the texture model and the conventional model by using multivariable logistic regression. The Radscore, which included the conventional_score, texture_score and combined_score was calculated via the logistic regression linear combination of the selected features weighted by their respective coefficients for each patient. Conventional_score, texture_score and combined_score were the corresponding formulas for calculating the above three models (conventional model, texture model and combined model).

Statistical analysis

The data were analysed using R software (version 3.6.1; http://www.Rproject.org) and MedCalc (ver. 10.3.0.0, MedCalc software). The Kolmogorov-Smirnov test was utilized to evaluate whether all sets of data adhered to a normal distribution. The t test or the Mann-Whitney *U* test was used to compare the differences between continuous variables, while the chi-squared test or Fisher's exact test was used for categorical variables. The agreement between different observers was evaluated through the application of the intraclass correlation coefficient (ICC). The strength of the association among the groups was assessed using the Pearson correlation coefficient, and r>0.8 indicated a high correlation. The Mann-Whitney *U* test was used to evaluate the difference in the Radscore between the *MET*ex14 skipping mutation group and the nonmutation group for each model. The three models were evaluated with 10-fold cross-validation. The performance of each model in predicting *MET*ex14 skipping mutation was evaluated by receiver operating characteristic curve (ROC) analysis. The DeLong test was used to compare differences among the three models. The benefit of the model was evaluated by decision curve analysis (DCA).

Results

Clinical and conventional CECT features

Fifty-six patients (40 males and 16 females; mean age, 58.14±8.7 years) were included in this study, of which 10 patients (17.9%) had *MET*ex14 skipping mutations.

The clinical features are listed in *Table 1*. T stage, long-axis diameter, and short-axis diameter were significantly different between the two groups (P=0.02, P=0.02, and P=0.01, respectively). The results of conventional CECT features are listed in *Table 2*. Pseudocapsular or annular enhancement was significantly different between the two groups (P=0.03). Mutations were found more frequently in (I) those who had smaller long- or short-axis diameters (P=0.02, P=0.01); (II) those who had lower T stages (stage I or II) (P=0.02); and (III) those with pseudocapsular or annular enhancement (P=0.03).

There are some implications for the diagnosis of PSC in conventional CECT features. In our study, PSCs were all solid masses (100%), mostly with some irregularities or irregular in shape (91.1%), with lobulation (92.9%), spiculation (92.9%), and poorly defined margins (83.9%). In some tumours, cystic changes or necrosis (39.3%) could be seen, and there may be obstructive changes (46.4%). The tumours were mostly heterogeneously enhanced (78.6%) on CECT, and some showed pseudocapsular or annular enhancement (19.6%). The overall CT value of PSC was 42.09 HU on average, which was lower than or equal to the back muscles at the same level (100%). Most of them had a pleural attachment (80.4%) or retraction (78.6%), and enlarged lymph nodes were seen in the mediastinum or hilum (44.6%). Meanwhile, bubble-like lucency (25%) was rare within the tumour, usually without pleural effusion (82.1%), no calcification (100%), and air bronchogram (100%).

Feature selection and model construction

All parameters showed good interobserver agreement (ICC >0.8). First, 44 features were retained after the correlation test. Second, 16 features were selected after univariate analysis. Finally, after multivariate logistic regression analysis, three features (wavelet_LowHighLow_GLDM_LowGrayLevelEmphasis, lbp_3D_m2_GLRLM_RunLengthNonUniformityNormalized, and wavelet_LowLowHigh_NGTDM_Strength) remained, and the corresponding

Table 1 Clinical data of the patients

Characteristic	All patients	*MET*ex14 skipping mutation	Non-mutation	P value
Sex				0.62
Female	16 (28.6)	4 (40.0)	12 (26.1)	
Male	40 (71.4)	6 (60.0)	34 (73.9)	
Age, years	58.14±8.74	60.30±9.13	57.67±8.68	0.34
Size, cm				
Long axis diameter	5.26±1.97	3.95±1.35	5.54±1.98	0.02
Short axis diameter	3.97±1.75	2.75±1.04	4.24±1.77	0.01
Smoking history				0.39
No	24 (42.9)	6 (60.0)	18 (39.1)	
Yes	32 (57.1)	4 (40.0)	28 (60.9)	
Location (distribution)				0.92
Central	26 (46.4)	4 (40.0)	22 (47.8)	
Peripheral	30 (53.6)	6 (60.0)	24 (52.2)	
Location (translobar)				0.94
No	48 (85.7)	9 (90.0)	39 (84.8)	
Yes	8 (14.3)	1 (10.0)	7 (15.2)	
Location (lobe)				0.57
Right upper lobe	9 (16.1)	2 (20.0)	7 (15.2)	
Right middle lobe	4 (7.1)	0	4 (8.7)	
Right lower lobe	11 (19.6)	1 (10.0)	10 (21.7)	
Left upper lobe	18 (32.1)	4 (40.0)	14 (30.4)	
Left lower lobe	14 (25.0)	3 (30.0)	11 (23.9)	
T stage				0.02
1	7 (12.5)	2 (20.0)	5 (10.9)	
2	21 (37.5)	7 (70.0)	14 (30.4)	
3	20 (35.7)	1 (10.0)	19 (41.3)	
4	8 (14.3)	0	8 (17.4)	
N stage				0.79
0	32 (57.1)	6 (60.0)	26 (56.5)	
1	11 (19.6)	2 (20.0)	9 (19.6)	
2	11 (19.6)	2 (20.0)	9 (19.6)	
3	2 (3.6)	0	2 (4.3)	
M stage				0.51
0	50 (89.3)	10 (100.0)	40 (87.0)	
1	6 (10.7)	0	6 (13.0)	

Table 1 (*continued*)

Table 1 (*continued*)

Characteristic	All patients	*MET*ex14 skipping mutation	Non-mutation	P value
AJCC stage				0.13
I	15 (26.8)	5 (50.0)	10 (21.7)	
II	18 (32.1)	2 (20.0)	16 (34.8)	
III	17 (30.4)	3 (30.0)	14 (30.4)	
IV	6 (10.7)	0	6 (13.0)	

Values are n (%) or mean ± SD. *MET*ex14 skipping, *MET* exon 14 skipping; AJCC, American Joint Committee on Cancer; SD, standard deviation.

Table 2 Conventional CECT imaging features of the patients

Features	All patients	*MET*ex14 skipping mutation	Non-mutation	P value
Shape				0.43
0	5 (8.9)	2 (20.0)	3 (6.5)	
1	24 (42.9)	4 (40.0)	20 (43.5)	
2	27 (48.2)	4 (40.0)	23 (50.0)	
Lobulation				0.14
0	4 (7.1)	2 (20.0)	2 (4.3)	
1	52 (92.9)	8 (80.0)	44 (95.7)	
Margin				0.92
0	47 (83.9)	9 (90.0)	38 (82.6)	
1	9 (16.1)	1 (10.0)	8 (17.4)	
Spiculation				0.95
0	4 (7.1)	1 (10.0)	3 (6.5)	
1	30 (53.6)	5 (50.0)	25 (54.4)	
2	22 (39.3)	4 (40.0)	18 (39.1)	
Bubble-like lucency				0.42
0	42 (75.0)	6 (60.0)	36 (78.3)	
1	14 (25.0)	4 (40.0)	10 (21.7)	
Cystic change or necrosis				0.68
0	34 (60.7)	5 (50.0)	29 (63.0)	
1	22 (39.3)	5 (50.0)	17 (37.0)	
Obstructive change				0.92
0	30 (53.6)	6 (60.0)	24 (52.2)	
1	26 (46.4)	4 (40.0)	22 (47.8)	

Table 2 (*continued*)

Table 2 (*continued*)

Features	All patients	*MET*ex14 skipping mutation	Non-mutation	P value
Enhancement heterogeneity				0.59
0	12 (21.4)	1 (10.0)	11 (23.9)	
1	44 (78.6)	9 (90.0)	35 (76.1)	
Pseudocapsular or annular enhancement				0.03
0	45 (80.4)	5 (50.0)	40 (87.0)	
1	11 (19.6)	5 (50.0)	6 (13.0)	
Overall CT value (HU)	42.09±15.18	38.30±16.65	42.91±14.91	0.39
CT value of back muscle (HU)	57.57±10.30	53.00±12.90	58.57±9.53	0.12
Enhancement relative ratio	0.74±0.25	0.72±0.26	0.74±0.24	0.83
Enhancement degree				0.67
0	33 (58.9)	7 (70.0)	26 (56.5)	
1	23 (41.1)	3 (30.0)	20 (43.5)	
Pleural attachment				0.68
0	11 (19.6)	2 (20.0)	9 (19.6)	
1	45 (80.4)	8 (80.0)	37 (80.4)	
Pleural retraction				0.76
0	12 (21.4)	2 (20.0)	10 (21.7)	
1	44 (78.6)	8 (80.0)	36 (78.3)	
Pleural effusion				0.24
0	46 (82.1)	10 (100.0)	36 (78.3)	
1	10 (17.9)	0	10 (21.7)	
Lymphadenopathy				0.98
0	31 (55.4)	6 (60.0)	25 (54.3)	
1	25 (44.6)	4 (40.0)	21 (45.7)	
None calcification	56 (100.0)	10 (100.0)	46 (100.0)	>0.99
None air bronchogram	56 (100.0)	10 (100.0)	46 (100.0)	>0.99
Solid texture	56 (100.0)	10 (100.0)	46 (100.0)	>0.99

Values are n (%) or mean ± SD. CECT, contrast-enhanced computed tomography; *MET*ex14 skipping, *MET* exon 14 skipping; CT, computed tomography; HU, Hounsfield unit; SD, standard deviation.

texture model was established.

For the conventional model, two features (pseudocapsular or annular enhancement and short-axis diameter) remained after multivariate logistic regression analysis, and the corresponding model was established.

The combined model integrated the conventional model and texture model and was constructed by using the conventional_score and texture_score. The details of the multivariate logistic regression models are listed in *Table 3*. Radscore was calculated as follows:

Conventional_score = –2.34 + (0.914 × pseudocapsular or annular enhancement – 1.58 × short-axis diameter);

Texture_score = 2.65 + (1.122 × wavelet_LowHighLow_GLDM_LowGrayLevelEmphasis + 1.388 × lbp_3D_m2_

Table 3 Multivariate logistic regression analysis

Model	OR	95% CI	β coefficient	P value	Model fit
Conventional model					0.184
Pseudocapsular or annular enhancement	2.493	1.214–5.121	0.914	0.01	
Short axis diameter	0.205	0.056–0.759	−1.58	0.02	
Texture model					0.643
wavelet_LowHighLow_GLDM_LowGrayLevelEmphasis	3.072	1.246–7.576	1.122	0.02	
lbp_3D_m2_GLRLM_RunLengthNonUniformityNormalized	4.001	1.221–13.141	1.388	0.02	
wavelet_LowLowHigh_NGTDM_Strength	2.280	1.048–4.959	0.824	0.04	
Combined model					0.643
Conventional_score	6.532	1.875–22.759	1.045	0.15	
Texture_score	8.552	2.186–33.456	1.574	0.04	

The goodness-of-fit of the logistic regression model was assessed using the Hosmer-Lemeshow test, and a model with P>0.05 was considered to be well fitted. OR, odds ratio; CI, confidence interval.

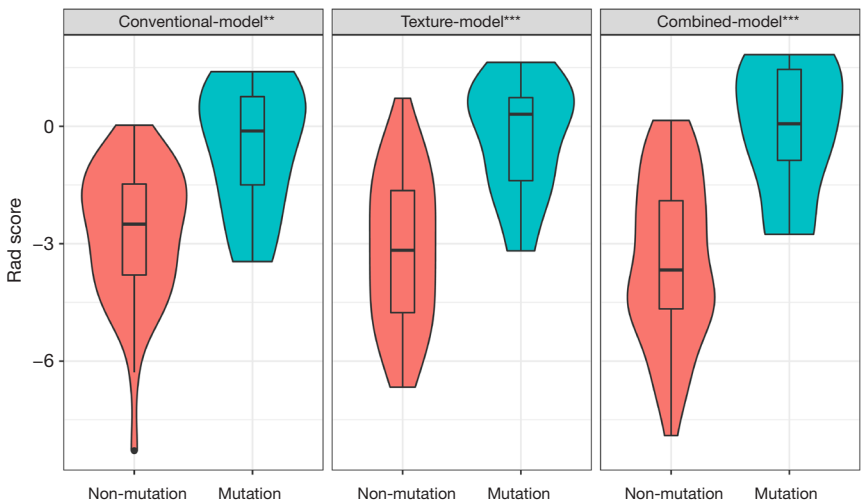

Figure 4 Distribution of the Radscore between the mutation and non-mutation groups in the four models. The density width represents the frequency of the Radscore. Within each box plot, the central line denotes the median of the Radscore, while the bottom and top edges of the box correspond to the first and third quartiles. The 'whiskers' extend to reflect the 95% confidence interval. **, P≤0.01; ***, P≤0.001.

GLRLM_RunLengthNonUniformityNormalized + 0.824 × wavelet_LowLowHigh_NGTDM_Strength);

Combined_score = −2.82 + (1.045 × conventional_score + 1.574 × texture_score).

Model comparison and evaluation

The differences in the Radscore between the *MET*ex14 skipping mutation group and the non-mutation group for each model are shown in *Figure 4*. The performance and ROC curves of each model are shown in *Table 4* and *Figure 5*. The AUCs of the conventional model, texture model, and combined model for predicting *MET*ex14 skipping mutation were 0.83 [95% confidence interval (CI): 0.669–0.985], 0.88 (95% CI: 0.766–0.994), and 0.89 (95% CI: 0.785–0.997), respectively. The DCA curves showed that all three models had better net returns than the None model and the All model over a wide range of risk thresholds between 0.1 and

Table 4 Model performance for predicting *MET*ex14 skipping mutation in PSC patients

Model	AUC	95% CI	Sensitivity (%)	Specificity (%)	Accuracy (%)
Conventional model	0.83	0.669–0.985	50.0	97.8	89.3
Pseudocapsular or annular enhancement					
Short axis diameter					
Texture model	0.88	0.766–0.994	80.0	73.9	75.0
wavelet_LowHighLow_GLDM_LowGrayLevelEmphasis					
lbp_3D_m2_GLRLM_RunLengthNonUniformityNormalized					
wavelet_LowLowHigh_NGTDM_Strength					
Combined model	0.89	0.785–0.997	70.0	82.6	80.4
Conventional_score					
Texture_score					

*MET*ex14 skipping, *MET* exon 14 skipping; PSC, pulmonary sarcomatoid carcinoma; AUC, area under the curve; CI, confidence interval.

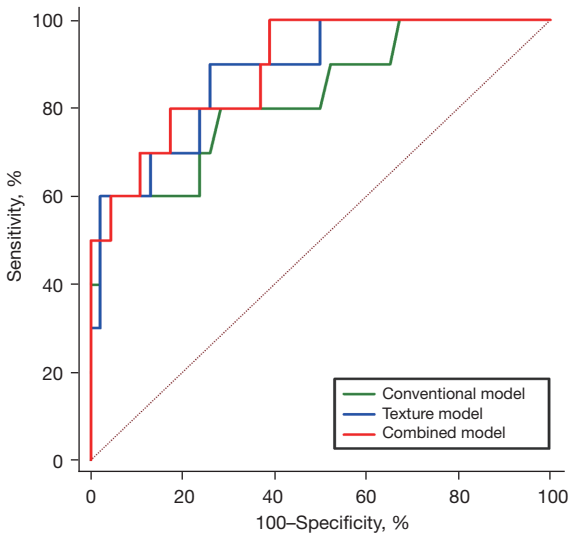

Figure 5 Comparison of the diagnostic performance of all models.

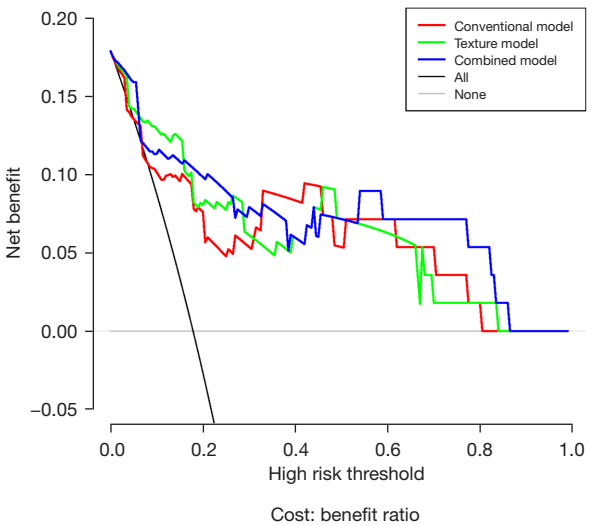

Figure 6 DCA of all models. The net benefit is determined by taking the proportion of true-positive patients and subtracting the proportion of false-positive patients, with this calculation adjusted according to the severity of the consequences of false positives and false negatives. The two extreme approaches of "treat all" and "treating none" are presented for comparative purposes. A clinical advantage is indicated when the decision curve demonstrates a net benefit that exceeds that of both reference strategies. DCA, decision curve analysis.

1.0 (*Figure 6*).

Discussion

This study aimed to predict *MET*ex14 skipping mutation status through clinical characteristics, conventional imaging features, and texture features, and it is also the PSC imaging study with the largest sample size. In this study, we constructed three models (conventional model, texture model, and combined model) based on CECT image-derived texture parameters, conventional features and clinical features to predict *MET*ex14 skipping mutation status in PSC patients. All the three models performed well, among which the combined model had a higher AUC

(0.89). Regarding the conventional features, mutations were found more frequently in (I) those who had a smaller long- or short-axis diameter (P=0.02, P=0.01); (II) those who had lower T stage (P=0.02); (III) those with pseudocapsular or annular enhancement (P=0.03).

PSC is a rare type of NSCLC with a high degree of malignancy, a poor prognosis, and limited efficacy in conventional surgical treatment (1). Fortunately, PSC has an "Achilles' heel": approximately 10% to 20% of patients have a *MET*ex14 skipping mutation. Some clinical trials have demonstrated that through targeted therapy (e.g., savolitinib, capmatinib, tepotinib and crizotinib), inhibition of *MET*ex14 mutations can bring clinical benefits. Therefore, the accurate judgement and early prediction of *MET*ex14 skipping mutation are significant for PSC. On the basis of previous research (12), our study included new PSC patients diagnosed in Cancer Hospital, Chinese Academy of Medical Sciences from 2017 to 2021, reviewed the CECT images of all patients, and then established three prediction models (conventional model, texture model, and combined model) to predict the *MET*ex14 skipping mutation status of PSC patients in a noninvasive way. From the clinical data, the proportion of *MET*ex14 skipping mutation in this study was 17.9%, which was basically consistent with that in previous studies (12,29). The median age of patients with PSC was 58 years, and the median tumour size (long-axis diameter) was 5.26 cm. The patients were more commonly male (71.4%), smokers (57.1%), and in stage 2–3 of the AJCC staging system (62.5%) at the time of initial diagnosis. These are consistent with previous studies (3,30,31). Our real-world clinical data help advance and complement PSC research. It is worth noting that in the conventional model, only the odds ratio (OR) value of short-axis diameter is less than 1, indicating a negative correlation with the predicted outcome. Indicating that the lesions in patients with mutations are relatively small, we suspect that the necrosis of smaller lesions is relatively mild, and the tumor parenchyma is relatively large, making it easier to detect tumor mutations. We also discussed imaging features about *MET*ex14 skipping mutation in previous studies, as shown in supplementary material (Appendix 1).

Texture analysis or radiomics can exploit the heterogeneity within the tumour to extract high-throughput image features from image data, and on this basis, the relationship between these deep image features and tumour gene expression or mutation can be analysed (32-34). Many studies have proven that the gene expression levels or gene mutations of lung cancer can be predicted by texture analysis or radiomics. Liu *et al.* (35), Jia *et al.* (24), Hong *et al.* (19), and Shiri *et al.* (36) predicted the EGFR mutation status; Weiss *et al.* (37) and Velazquez *et al.* (38) predicted the KRAS mutation status; and Kim *et al.* (39) and Choi *et al.* (40) predicted the ALK mutation status. At the same time, adding clinical or conventional imaging features on the basis of texture analysis or radiomics is more helpful for the diagnosis and prediction of the model. Song *et al.* (25) used radiomics to predict ALK mutation status in lung adenocarcinoma and added clinical and conventional CT features on this basis, which ultimately improved the diagnostic performance of the primary model (AUC =0.83–0.88, P=0.01). There are many similar studies that incorporated clinical, conventional imaging features and texture features (41-43). Three prediction models were established in our study, all of which can predict *MET*ex14 skipping mutation status to a certain extent. Among them, the combined model performed the best. Three features were incorporated into the construction of the texture model, including two wavelet transform features. The wavelet transform is particularly suited for analyzing nonstationary signals and elementary functions that exhibit variation in both the frequency domain and spatial extent. It is crafted to deliver superior frequency resolution for the low-frequency elements, representing the overall image intensity, and excellent temporal resolution for the high-frequency elements, which correspond to the image's edge details (44). These three features all can reflect the tumour's intensity and textural features surrounding and within the high-intensity CT voxels, providing the possibility to predict gene mutations.

This study has some limitations. First, these data are based on a single-centre retrospective study, which will inevitably lead to selection bias. The number of cases with *MET*ex14 skipping mutations included in the study was relatively small, which may cause overfitting of the model. Nonetheless, this study is the largest imaging study of PSC ever. Second, the VOI and conventional imaging features were manually determined. These human factors may cause errors in feature extraction and conventional feature judgement. In future work, we hope to build a more advanced system by referring to the work of Tomassini *et al.* (45), to determine the *MET*ex14 skipping mutation by segmentation free CT scans, coupled with an on-cloud decision-support system. Third, due to the small amount

of data in this study, we did not have a validation group to validate the model.

Conclusions

In conclusion, our findings highlight the feasibility of noninvasively predicting *MET*ex14 skipping mutations in PSC patients using an integrated model that combines clinical and conventional CECT features and texture features.

Acknowledgments

We would like to thank the investigators at all participating study sites.
Funding: This work was supported by grants from National Natural Science Foundation of China (No. 22272203).

Footnote

Reporting Checklist: The authors have completed the TRIPOD reporting checklist. Available at https://tlcr.amegroups.com/article/view/10.21037/tlcr-24-56/rc

Data Sharing Statement: Available at https://tlcr.amegroups.com/article/view/10.21037/tlcr-24-56/dss

Peer Review File: Available at https://tlcr.amegroups.com/article/view/10.21037/tlcr-24-56/prf

Conflicts of Interest: All authors have completed the ICMJE uniform disclosure form (available at https://tlcr.amegroups.com/article/view/10.21037/tlcr-24-56/coif). Y.W. is an employee of GE Healthcare. The other authors have no conflicts of interest to declare.

Ethical Statement: The authors are accountable for all aspects of the work in ensuring that questions related to the accuracy or integrity of any part of the work are appropriately investigated and resolved. The study was conducted in accordance with the Declaration of Helsinki (as revised in 2013). The Ethical Committee of the Cancer Hospital, Chinese Academy of Medical Sciences approved this study (No. 18-224/1782) and waived the requirement for obtaining informed consent from patients, as data were de-identified, involving no potential risk to patients and no link between the patients and researchers.

References

1. Lu S, Fang J, Li X, et al. Once-daily savolitinib in Chinese patients with pulmonary sarcomatoid carcinomas and other non-small-cell lung cancers harbouring MET exon 14 skipping alterations: a multicentre, single-arm, open-label, phase 2 study. Lancet Respir Med 2021;9:1154-64.
2. Yang Z, Xu J, Li L, et al. Integrated molecular characterization reveals potential therapeutic strategies for pulmonary sarcomatoid carcinoma. Nat Commun 2020;11:4878.
3. Zeng Q, Li J, Sun N, et al. Preoperative systemic immune-inflammation index predicts survival and recurrence in patients with resected primary pulmonary sarcomatoid carcinoma. Transl Lung Cancer Res 2021;10:18-31.
4. Vieira T, Girard N, Ung M, et al. Efficacy of first-line chemotherapy in patients with advanced lung sarcomatoid carcinoma. J Thorac Oncol 2013;8:1574-7.
5. Ung M, Rouquette I, Filleron T, et al. Characteristics and Clinical Outcomes of Sarcomatoid Carcinoma of the Lung. Clin Lung Cancer 2016;17:391-7.
6. Maemondo M, Inoue A, Kobayashi K, et al. Gefitinib or chemotherapy for non-small-cell lung cancer with mutated EGFR. N Engl J Med 2010;362:2380-8.
7. Garon EB, Rizvi NA, Hui R, et al. Pembrolizumab for the treatment of non-small-cell lung cancer. N Engl J Med 2015;372:2018-28.
8. Herbst RS, Baas P, Kim DW, et al. Pembrolizumab versus docetaxel for previously treated, PD-L1-positive, advanced non-small-cell lung cancer (KEYNOTE-010): a randomised controlled trial. Lancet 2016;387:1540-50.
9. Pécuchet N, Vieira T, Rabbe N, et al. Molecular classification of pulmonary sarcomatoid carcinomas suggests new therapeutic opportunities. Ann Oncol 2017;28:1597-604.
10. Liu X, Jia Y, Stoopler MB, et al. Next-Generation Sequencing of Pulmonary Sarcomatoid Carcinoma Reveals

High Frequency of Actionable MET Gene Mutations. J Clin Oncol 2016;34:794-802.
11. Vuong HG, Ho ATN, Altibi AMA, et al. Clinicopathological implications of MET exon 14 mutations in non-small cell lung cancer - A systematic review and meta-analysis. Lung Cancer 2018;123:76-82.
12. Li Y, Gao L, Ma D, et al. Identification of MET exon14 skipping by targeted DNA- and RNA-based next-generation sequencing in pulmonary sarcomatoid carcinomas. Lung Cancer 2018;122:113-9.
13. Wolf J, Seto T, Han JY, et al. Capmatinib in MET Exon 14-Mutated or MET-Amplified Non-Small-Cell Lung Cancer. N Engl J Med 2020;383:944-57.
14. Paik PK, Felip E, Veillon R, et al. Tepotinib in Non-Small-Cell Lung Cancer with MET Exon 14 Skipping Mutations. N Engl J Med 2020;383:931-43.
15. Drilon A, Clark JW, Weiss J, et al. Antitumor activity of crizotinib in lung cancers harboring a MET exon 14 alteration. Nat Med 2020;26:47-51.
16. Li X, Wu D, Liu H, et al. Pulmonary sarcomatoid carcinoma: progress, treatment and expectations. Ther Adv Med Oncol 2020;12:1758835920950207.
17. Boland JM, Mansfield AS, Roden AC. Pulmonary sarcomatoid carcinoma-a new hope. Ann Oncol 2017;28:1417-8.
18. Yang ZY, Liu ZY, Mu CY, et al. Letter: Exploring the accuracy of biopsy in diagnosis of pulmonary sarcomatoid carcinoma. Lung Cancer 2021;151:97.
19. Hong D, Xu K, Zhang L, et al. Radiomics Signature as a Predictive Factor for EGFR Mutations in Advanced Lung Adenocarcinoma. Front Oncol 2020;10:28.
20. Sosa E, D'Souza G, Akhtar A, et al. Racial and socioeconomic disparities in lung cancer screening in the United States: A systematic review. CA Cancer J Clin 2021;71:299-314.
21. Watari N, Yamaguchi K, Terada H, et al. Characteristic computed tomography features in mesenchymal-epithelial transition exon14 skipping-positive non-small cell lung cancer. BMC Pulm Med 2022;22:260.
22. Digumarthy SR, Mendoza DP, Zhang EW, et al. Clinicopathologic and Imaging Features of Non-Small-Cell Lung Cancer with MET Exon 14 Skipping Mutations. Cancers (Basel) 2019;11:2033.
23. Le NQK, Kha QH, Nguyen VH, et al. Machine Learning-Based Radiomics Signatures for EGFR and KRAS Mutations Prediction in Non-Small-Cell Lung Cancer. Int J Mol Sci 2021;22:9254.
24. Jia TY, Xiong JF, Li XY, et al. Identifying EGFR mutations in lung adenocarcinoma by noninvasive imaging using radiomics features and random forest modeling. Eur Radiol 2019;29:4742-50.
25. Song L, Zhu Z, Mao L, et al. Clinical, Conventional CT and Radiomic Feature-Based Machine Learning Models for Predicting ALK Rearrangement Status in Lung Adenocarcinoma Patients. Front Oncol 2020;10:369.
26. Agazzi GM, Ravanelli M, Roca E, et al. CT texture analysis for prediction of EGFR mutational status and ALK rearrangement in patients with non-small cell lung cancer. Radiol Med 2021;126:786-94.
27. Lambin P, Rios-Velazquez E, Leijenaar R, et al. Radiomics: extracting more information from medical images using advanced feature analysis. Eur J Cancer 2012;48:441-6.
28. Zwanenburg A, Vallières M, Abdalah MA, et al. The Image Biomarker Standardization Initiative: Standardized Quantitative Radiomics for High-Throughput Image-based Phenotyping. Radiology 2020;295:328-38.
29. Han S, Fang J, Lu S, et al. Response and acquired resistance to savolitinib in a patient with pulmonary sarcomatoid carcinoma harboring MET exon 14 skipping mutation: a case report. Onco Targets Ther 2019;12:7323-8.
30. Rahouma M, Kamel M, Narula N, et al. Pulmonary sarcomatoid carcinoma: an analysis of a rare cancer from the Surveillance, Epidemiology, and End Results database. Eur J Cardiothorac Surg 2018;53:828-34.
31. Mehrad M, Roy S, LaFramboise WA, et al. KRAS mutation is predictive of outcome in patients with pulmonary sarcomatoid carcinoma. Histopathology 2018;73:207-14.
32. van Timmeren JE, Cester D, Tanadini-Lang S, et al. Radiomics in medical imaging-"how-to" guide and critical reflection. Insights Imaging 2020;11:91.
33. Bodalal Z, Trebeschi S, Nguyen-Kim TDL, et al. Radiogenomics: bridging imaging and genomics. Abdom Radiol (NY) 2019;44:1960-84.
34. Liu Z, Wu K, Wu B, et al. Imaging genomics for accurate diagnosis and treatment of tumors: A cutting edge overview. Biomed Pharmacother 2021;135:111173.
35. Liu Y, Kim J, Balagurunathan Y, et al. Radiomic Features Are Associated With EGFR Mutation Status in Lung Adenocarcinomas. Clin Lung Cancer 2016;17:441-448.e6.
36. Shiri I, Maleki H, Hajianfar G, et al. Next-Generation Radiogenomics Sequencing for Prediction of EGFR and KRAS Mutation Status in NSCLC Patients Using Multimodal Imaging and Machine Learning Algorithms. Mol Imaging Biol 2020;22:1132-48.

37. Weiss GJ, Ganeshan B, Miles KA, et al. Noninvasive image texture analysis differentiates K-ras mutation from pan-wildtype NSCLC and is prognostic. PLoS One 2014;9:e100244.
38. Rios Velazquez E, Parmar C, Liu Y, et al. Somatic Mutations Drive Distinct Imaging Phenotypes in Lung Cancer. Cancer Res 2017;77:3922-30.
39. Kim TJ, Lee CT, Jheon SH, et al. Radiologic Characteristics of Surgically Resected Non-Small Cell Lung Cancer With ALK Rearrangement or EGFR Mutations. Ann Thorac Surg 2016;101:473-80.
40. Choi CM, Kim MY, Hwang HJ, et al. Advanced adenocarcinoma of the lung: comparison of CT characteristics of patients with anaplastic lymphoma kinase gene rearrangement and those with epidermal growth factor receptor mutation. Radiology 2015;275:272-9.
41. Xiao G, Hu YC, Ren JL, et al. MR imaging of thymomas: a combined radiomics nomogram to predict histologic subtypes. Eur Radiol 2021;31:447-57.
42. Seo M, Choi MH, Lee YJ, et al. Evaluating the added benefit of CT texture analysis on conventional CT analysis to differentiate benign ovarian cysts. Diagn Interv Radiol 2021;27:460-8.
43. Ye R, Weng S, Li Y, et al. Texture Analysis of Three-Dimensional MRI Images May Differentiate Borderline and Malignant Epithelial Ovarian Tumors. Korean J Radiol 2021;22:106-17.
44. Bhattacharjee S, Kim CH, Park HG, et al. Multi-Features Classification of Prostate Carcinoma Observed in Histological Sections: Analysis of Wavelet-Based Texture and Colour Features. Cancers (Basel) 2019;11:1937.
45. Tomassini S, Falcionelli N, Bruschi G, et al. On-cloud decision-support system for non-small cell lung cancer histology characterization from thorax computed tomography scans. Comput Med Imaging Graph 2023;110:102310.

Cite this article as: Miao L, Qiu T, Li Y, Li J, Jiang X, Liu M, Zhang X, Jiang J, Zhang H, Wang Y, Li X, Ying J, Li M. Predicting *MET* exon 14 skipping mutation in pulmonary sarcomatoid carcinoma by whole-tumour texture analysis combined with clinical and conventional contrast-enhanced computed tomography features. Transl Lung Cancer Res 2024;13(6):1232-1246. doi: 10.21037/tlcr-24-56